J Nanostruct 14(2): 411-426, Spring 2024

RESEARCH PAPER

Preparation, Spectral Characterization, Antimicrobial and Cytotoxic Studies of some Transition Metal Nanocomplexes of a Novel Azo Derivative Formed from 2-Amino -5- Methylthiazol

Suha Hassan Majhool *, Azal Shakir Waheeb, and Masar Ali Awad

Department of Chemistry, College of Science, University, Al- Muthanna, Iraq

ARTICLE INFO

Article History:
Received 04 February 2024
Accepted 26 March 2024
Published 01 April 2024

Keywords:
Metal ions
Nanocomplexes
NMR
SEM
XRD

ABSTRACT

The present investigation delineates the synthetic procedure employed for the production of 2-[2'-(5-methylthiazolyl)azo]-5,6-Dimethyl benzoimidazole (L1) and its corresponding silver(I) complex (C1) as well as gold(III) complex (C2). The ligand and the complexes underwent comprehensive characterization using a range of analytical techniques including FT-IR spectroscopy, nuclear magnetic resonance ^{1}H-NMR spectroscopy, 13C-NMR spectroscopy, mass spectrometry, Elemental Analysis (CHNS), molar conductivity measurements, X-Ray diffraction analysis, field emission scanning electron microscopy (FE-SEM), and magnetic susceptibility measurements. The antibacterial and antifungal properties of these compounds were assessed, revealing that the synthesized compounds demonstrated superior efficacy against bacteria in comparison to conventional antibacterial medications. Nevertheless, their efficacy against fungal pathogens was observed to be comparatively diminished in comparison to conventional antifungal medications. Based on the findings from molecular docking investigations, the synthesized compounds were evaluated for their binding affinity towards the kinase domain of human DDR1 in conjunction with the pancreatic cancer-associated protein. Furthermore, the L1 compound and C1 compound were subjected to evaluation in terms of their anti-cancer efficacy against a specific pancreatic carcinoma cell line (TP-53) utilizing the MTT assay. The experimental results have revealed that the examined compounds exhibit noteworthy anti-cancer properties, thereby implying their prospective utilization as auspicious contenders for subsequent advancement as anti-neoplastic agents.

How to cite this article
Majhool S H., Waheeb A. S, Awad M A. Preparation, Spectral Characterization, Antimicrobial and Cytotoxic Studies of some Transition Metal Nanocomplexes of a Novel Azo Derivative Formed from 2-Amino -5- Methylthiazol. J Nanostruct, 2024; 14(2):411-426. DOI: 10.22052/JNS.2024.02.005

INTRODUCTION

Coordination compounds, renowned for their remarkable utility in metallurgical processes, industrial catalysis, and analytical reagents [1], have garnered significant attention in these domains. Electroplating, textile dyeing, and pharmaceutical chemistry frequently employ a diverse array of coordination complexes [2,3]. Azo dyes, make up a substantial fraction, approximately 70%, of the entire spectrum of industrial dyes

* *Corresponding Author Email: suhahassan002@gmail.com*

[4, 5]. The salient feature of these compounds resides in their functional moieties (-N=N-), which encompass two symmetrical and/or asymmetrical identical or non-azo alkyl or aryl substituents [6]. Heterocyclic compounds comprising sulfur and nitrogen atoms have been employed as highly adaptable and distinctive frameworks in the realm of experimental drug design [7-9]. Thiazolyl azo compounds possess a distinctive amalgamation of nitrogen and sulfur, which endows them with remarkable coordination capabilities. This enables them to engage with a wide range of metal ions and facilitates the creation of enduring and discriminating complexes. Consequently, these compounds exhibit exceptional efficacy in a multitude of analytical applications [10-12].

Thiazole compounds, being a crucial class of organic compounds, exhibit significant versatility across diverse industrial sectors. Dyes play a crucial role as dyeing agents within various industries, including leather, polymer, paint, and coating industries. Furthermore, within the realm of medicinal chemistry, there has been a notable surge in interest in Metallodrugs. These compounds have emerged as pivotal entities in the advancement of innovative therapeutic agents that possess metal-based frameworks. A thorough investigation of the coordination chemistry of these complexes is imperative to ensure their biocompatibility, safety, and efficacy as potential therapeutic agents. Several crucial factors, including the selection of an appropriate metal ion, consideration of oxidation states, assessment of stability, and careful selection of suitable ligands, must be meticulously taken into account [13-15]. This resulted in the emergence of numerous molecular entities incorporating transition metal ions, which have found utility in the realm of medicinal applications.

The ongoing investigation is centered on the synthesis and characterization of L1, as well as its complexes (C1 and C2) with Ag(I) and Au(III) metals, correspondingly. The investigation also delves into the potential antimicrobial and anticancer attributes exhibited by these synthesized compounds. In order to acquire a comprehensive understanding of the molecular architectures, a multitude of analytical methodologies have been employed, encompassing elemental analyses such as CHNS, Fourier Transform Infrared Spectroscopy (FT-IR), Nuclear Magnetic Resonance (NMR) spectroscopy utilizing both proton (^{1}H) and carbon-13 (^{13}C) nuclei, X-ray crystallography, Field Emission Scanning Electron Microscopy (FE-SEM), molar conductance measurements, and magnetic moment measurements.

MATERIALS AND METHODS

Chemicals and Reagent

A diverse array of chemical compounds and reagents were employed throughout the synthetic procedures, and they were utilized without undergoing subsequent purification steps. The aforementioned premium-grade chemical compounds were procured from esteemed commercial vendors. The chemical compounds present in the provided list include 2-amino-5-methylthiazole, 5-6-dimethyl benzimidazole, sodium nitrite, $AgNO_3$, $HAuCl_4 \cdot 4H_2O$, 2-(4,5-dimethylthiazol-2-yl)-3,5-diphenyl-2H-tetrazol-3-ium bromide, sodium hydroxide, dimethyl sulfoxide, ethanol, methanol, $CaCl_2$, HCl, deionized water, novobiocin, cycloheximide, and Mueller Hinton agar.

Physical Measurements

The ligand (L1) and its corresponding complexes C1 and C2 underwent elemental analyses utilizing the E.A 300 (CHNS/O) element analyzer. The Nuclear Magnetic Resonance (NMR) spectra, encompassing both proton (^{1}H) and carbon-13 (^{13}C) nuclei, were acquired utilizing a Bruker 500 MHz spectrophotometer. The measurements were conducted in a solvent of deuterated dimethyl sulfoxide (DMSO-d_6), with tetramethyl silane serving as the internal standard. The mass spectrometric calculations of L1 and C2 were conducted employing a Schimadzu Agilent Technologies 5973C mass spectrometer operating at an energy level of 70 electron volts (eV). UV spectra were acquired in an ethanol (C_2H_5OH) solvent using a T80-PG double-beam UV-Visible spectrophotometer. The vibrational spectrum was acquired utilizing a Schimadzu 8400 S instrument. In order to discern the metallic constituents of Ag(I) and Au(II) complexes, we utilized a Schimadzu AA 6300 atomic absorption spectrophotometer. FE-SEM images were acquired employing a ZEIS SEM 3200 instrument operating at an accelerating voltage of 30 kilovolts. Magnetic measurements were performed utilizing a magnetic susceptibility balance model (MSB/MKIC), employing the Faraday technique, Pascal constant, and diamagnetic corrections. The determination of the compounds'

melting points was conducted utilizing the SMP Stuart instrument. The pH measurements were acquired utilizing a Phillips PW 9421 instrument.

Synthetic process of 2-[2'-(5- methylthiazolyl)azo]-5-,6- Di methyl benzoimidazol (L1)

The ligand L1 was synthesized via a modification of the previously established methodology documented in our laboratory's prior publications [16,17] (Fig. 1). The novel ligand, L1, was synthesized through the dissolution of 2-amino-5-methylthiazole (1.30 g, 10 mmol) in a solution containing 5 mL of hydrochloric acid (HCl) and 30 mL of distilled water. The diazotization process was successfully accomplished by employing a controlled cooling technique, reducing the solution's temperature to a range of 0–5°C. Subsequently, a chilled aqueous mixture containing sodium nitrite (0.9 g, 10 mmol) was meticulously introduced into the solution in a gradual and incremental manner. The diazotized product was subsequently subjected to a reaction with 5,6-dimethyl benzimidazole (1.46 g, 10 mmol), which was subsequently introduced into a solution consisting of 35 mL of C_2H_5OH and 15 mL of a 10% sodium hydroxide solution. The coupling reaction was conducted under cryogenic conditions using an ice bath maintained at a temperature of 0°C for a duration of 1 hour. Upon the culmination of the chemical transformation, the amalgamation underwent the process of filtration, whereby the ensuing solid precipitate was subjected to meticulous rinsing iterations employing distilled water. Subsequently, the precipitate was subjected to recrystallization, a procedure encompassing its dissolution in absolute ethanol, followed by the facilitation of crystal reformation. Ultimately, the ligand underwent a desiccation process within the confines of a desiccator, where it was subjected to a temperature of 50°C for a duration of several hours.

Synthesis of Ag(I) (C_1) and Au(III) (C_2) Complexes

Metal chelates were successfully synthesized employing a precisely measured quantity of 0.2713 g, equivalent to 1 mmole, of the ligand L1, which was meticulously dissolved in 50 mL of heated ethanol. In order to synthesized the metal complexes C1 and C2, ethanoic solutions of L1 were individually combined with stirring in the presence of 0.1698 g (1mmol) of $AgNO_3$ and 0.5179 g (1mmol) of $HAuCl_4 \cdot 4H_2O$, respectively. The metal ions were solvated in the minimal volume of buffer solution (NH_4OAc) necessary, ensuring the pH was optimized for each specific metal salt. The mixture underwent reflux for a duration of 60 minutes, followed by an extended period of overnight rest. Following the completion of the reaction period, the resulting products were obtained in the solid state and subsequently

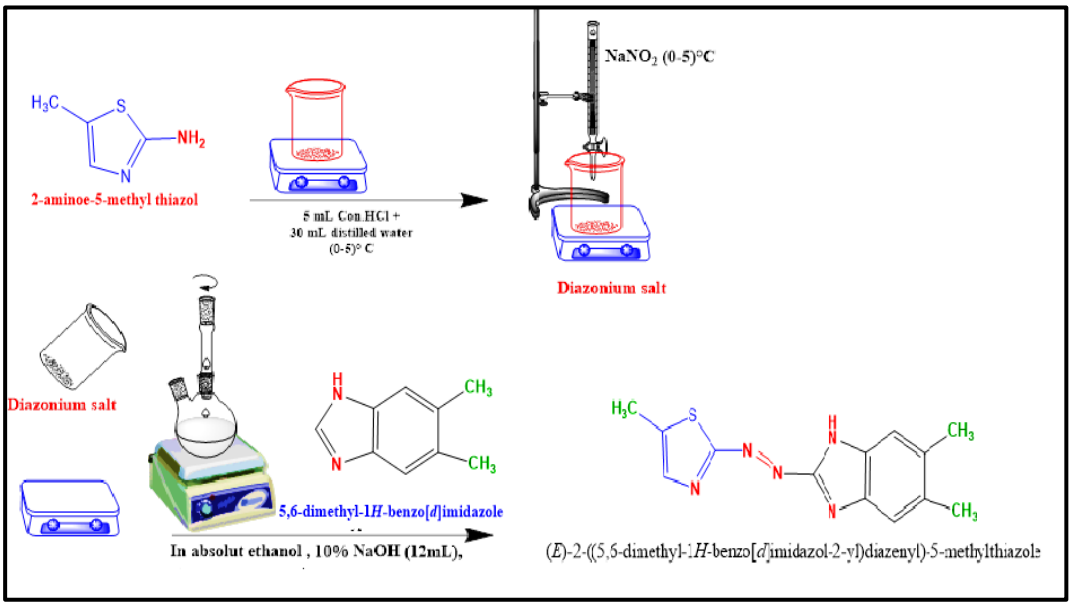

Fig. 1. Synthetic path of azo dye ligand 2-[2'-(5- methylthiazolyl)azo]- 5-,6- Di methyl benzoimidazol (5-MTADMBI).

isolated through the process of filtration. The isolated compounds underwent a thorough rinsing process using water until achieving a colorless appearance. Subsequently, a supplementary wash was performed utilizing 10 mL of a hot 50% aqueous solution of C_2H_5OH to ensure the complete removal of any residual unreacted constituents. Subsequently, the aforementioned compounds underwent vacuum drying within the confines of a desiccator, utilizing anhydrous calcium chloride as the desiccant, for an extended duration of time. A comprehensive elemental analysis was conducted on the (CHNS) compound, and the accompanying characteristics of the resultant complexes have been succinctly outlined in Table 1, as depicted in Fig. 2.

RESULTS AND DISCUSSION

The presence of the ligand L1 was visually detected in the crystalline state, exhibiting a characteristic brown hue. Upon the coordination of metal ions with ligands, the ensuing metal chelate complexes manifested alterations in their optical properties, leading to observable changes in coloration. Furthermore, these complexes were observed to adopt crystalline structures. All the specimens exhibited limited solubility in aqueous media while demonstrating solubility in DMF, DMSO, EtOH, and MeOH, and were observed to exist in solid form under ambient conditions. The experimental findings have elucidated that the stoichiometry between the metal and ligand in these complexes is precisely [M: L] 1:1, as

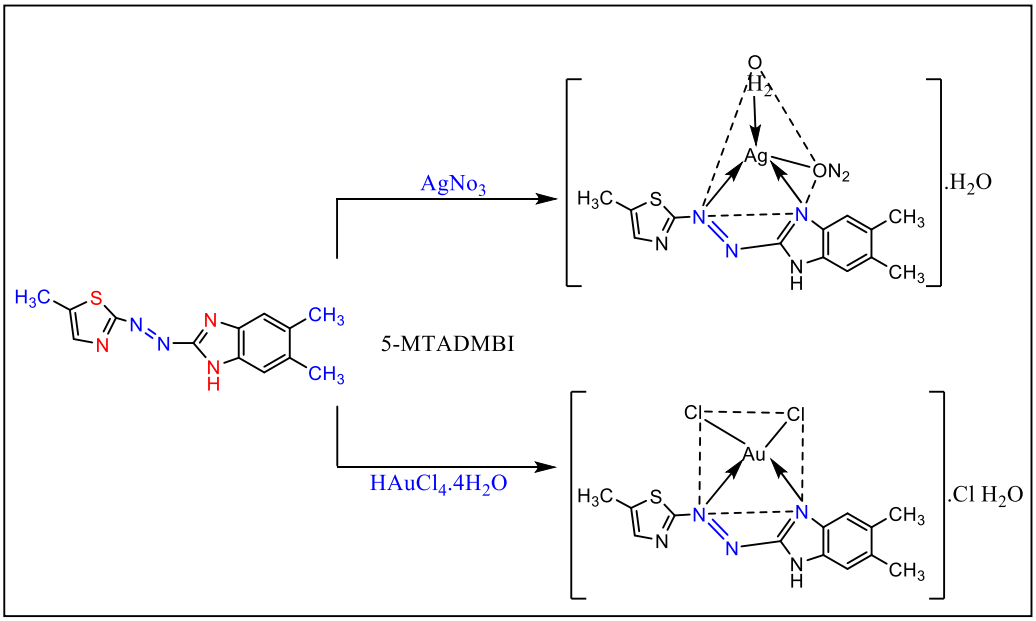

Fig. 2. Syntheses of metal chelates.

Table 1. Analytical and physical data of the ligand (5-MTADMBI) and its complexes.

Compound	Color	m.p °C	Yield (%)	M.f (M.wt)	Elemental analysis (%): Found (Calculated)				
					C%	H%	N%	S%	M%
Ligand LH=(5-MTADMBI)	Brown crystal	128	74	$C_{13}H_{13}N_5S$ 271.34	58.14 (57.54)	5.98 (4.83)	26.11 (25.81)	11.91 (11.82)	...
Ag (I) complex	Dark brown	206	69	$C_{13}H_{17}AgN_7O_2S$ 443.25	36.41 (35.23)	4.88 (3.87)	21.75 (22.12)	8.11 (7.23)	(24.34)
Au (III) complex	Orange	184	70	$C_{14}H_{17}AuCl_3N_5S$ 589.7	30.03 (28.51)	3.21 (2.90)	12.79 (11.87)	6.22 (5.43)	(33.40)

Table 2. Stability constant values (β and Logβ), maximum wavelength, optimal concentration and molar conductivity of metal chelate complexes.

LH=(5-MTADMBI) λ_{max} = 387nm Conc.= 1.25x10^{-4}M	Metal ion	Optimal Conc. X 10^{-4}	λmax (nm)	(β) L^2.M^{-2}	Log β	Molar absorptivity × 10^3 (ε) L. mol^{-1} cm^{-1}	Molar Conductivity S. cm^2 mol^{-1}
	Ag(I)	1.50	587 nm	2.4x10^4	4.38	5.161	13.67
	Au(III)	2.00	598 nm	3.5x10^4	4.55	1.383	39.27

reported in reference [18]. The elemental analysis of the synthesized compound corroborated the anticipated chemical formulas. Table 1 presents the elemental analyses, melting temperatures, and yields of the compounds.

Molar conductivity and stability constant determination

At the temperature commonly found within a laboratory setting, the solution of C1 dissolved in ethanol displays a molar conductance value of 13.67 S.cm^2.mol^{-1}. The observed value is situated within the spectrum of non-electrolytes, thereby suggesting that the complex exhibits a diminished degree of ionic character. The experimental evidence indicates that the compound denoted as C1 lacks any ions in its immediate vicinity, referred to as the coordination sphere. However, it is plausible that these ions could either be absent or present within the coordination sphere. The aforementioned observation was corroborated by means of chemical analysis, wherein the introduction of silver nitrate solution to the complex did not yield any precipitated chloride ions. In contrast, it is noteworthy that the C2 compound exhibits a significantly elevated molar conductivity measurement of 39.27 (S.cm^2.mol^{-1}), thereby suggesting its propensity to function as a 1:1 electrolyte and thereby affirming its ionic nature. Upon the introduction of an aqueous solution of Silver nitrate to the C2, a discernible white precipitate materialized, thereby affirming

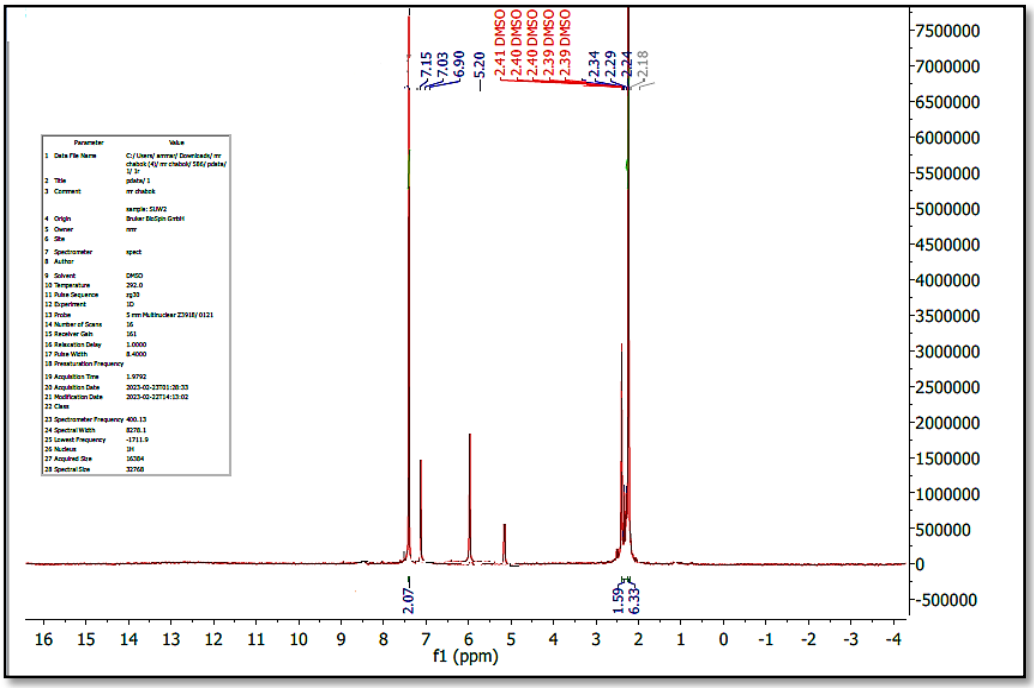

Fig. 3. Spectrum of Azo dye ligand by ^{1}H-NMR

the presence of chloride ions in the extra coordination environment. In order to ascertain the stability of the complexes, absorbance measurements were acquired for a combination of L1 and the corresponding metals at a designated wavelength (λ_{max}) and optimal concentrations. Based on the provided data, the stability constant (β) of the compounds was determined through rigorous calculations and analysis. Table 2 displays the recorded values of stability constants.

^{1}H-NMR spectra

The proton nuclear magnetic resonance (^{1}H-NMR) spectra of L1 and C2 were acquired using a Bruker 500 megahertz (MHz) spectrophotometer, employing dimethyl sulfoxide-d6 (DMSO-d_6) as the

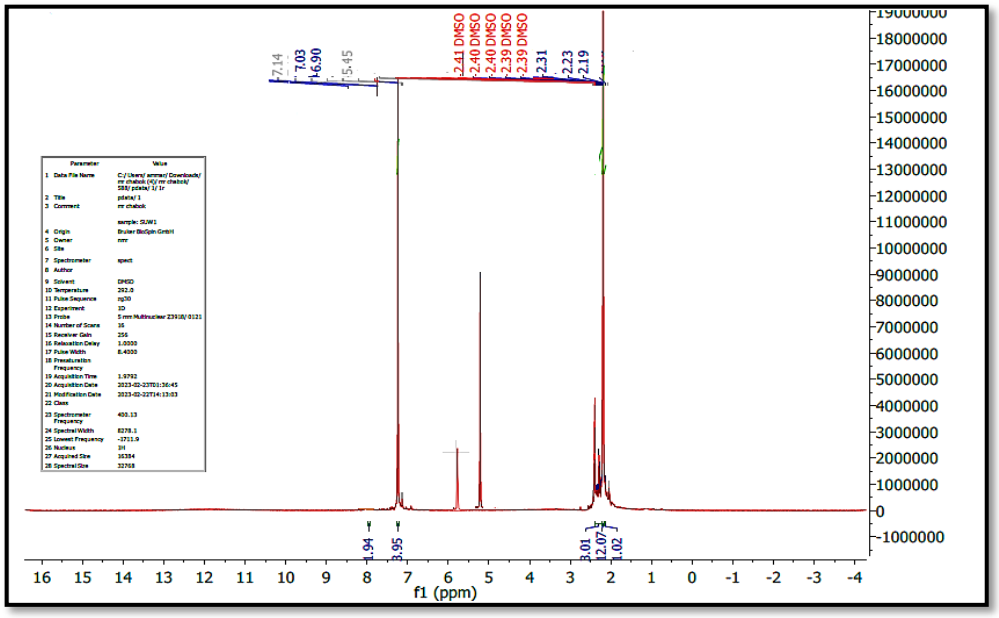

Fig. 4. ^{1}H NMR Spectrum of Au(III)-Complex

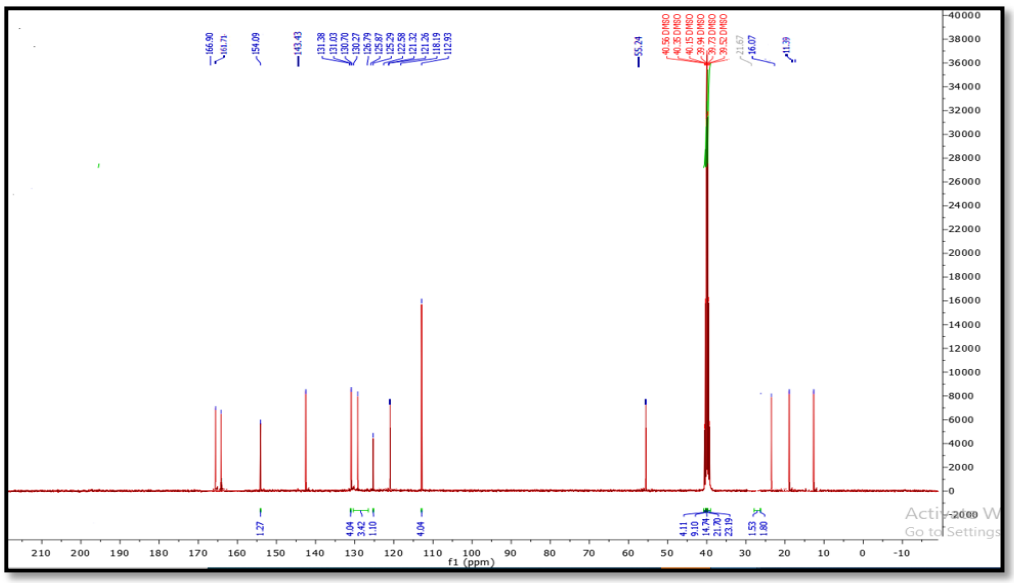

Fig. 5. ^{13}C NMR spectrum of ligand (5-MTADMBI)

solvent. The spectral analysis of L1 revealed the presence of characteristic peaks at δ=7.14 ppm, which can be assigned to the NH moiety within the imidazole group, and δ=2.19 ppm, indicative of the methyl group within the imidazole ring. The aromatic hydrogens in the imidazole group exhibited a signal spanning from δ=5.45 to 6.90 ppm, while the proton of the methyl group and the proton in the thiazol ring were assigned signals at δ=2.31 and 7.03 ppm, respectively. Furthermore, an observable singlet peak was observed at a chemical shift of δ=2.23 ppm, providing evidence for the existence of methyl groups within the benzoimidazole ring. It is of utmost significance to acknowledge the presence of a solvent peak, which manifested as a singlet at a chemical shift of δ=2.39-2.41 ppm [21].

On the other hand, within the ^{1}H -NMR spectrum of C2, an observable resonance was identified at a chemical shift of δ=7.15 parts per million (ppm), indicative of the presence of the NH moiety within the imidazole ring. The aromatic protons in the benzoimidazole ring were assigned to signals spanning from δ=5.20 to 6.90 ppm. Additionally, the methyl group in the thiazole ring was associated with a signal at δ=2.34 ppm, while the proton in the thiazole ring was specified to resonate at δ=7.03 ppm. Moreover, a singlet signal manifested at 2.24 parts per million (ppm), thereby corroborating the existence of methyl moieties within the benzoimidazole framework. Analogous to the unbound ligand, the solvent peak was detected at a chemical shift of δ=2.39-2.41 ppm [22]. Figs. 3 and 4 depict the ^{1}H-NMR spectra of the synthesized compounds.

^{13}C NMR spectra

The L1 compound was subjected to analysis utilising ^{13}C-NMR spectroscopy, wherein distinct signals were observed, indicative of the presence of diverse carbon atom species [23]. The observed ^{13}C NMR spectrum displayed a range of distinct signals at chemical shifts of 166.90, 161.71, 154.09, 143.43, 131.38, 131.03, 122.58, 118.19, 112.93, 55.24, 21.67, 16.07, and 11.39 parts per million (ppm). These signals correspond to the carbon atoms situated at positions C2, C12, C16, C4, C15, C5, C17, C14, C9, C11, C18, C19, and C6, respectively, as reported in reference [24]. The ^{13}C-NMR spectra of L1 have been acquired and are depicted in Fig. 5.

Mass spectral studies

Mass spectrometry is an indispensable analytical methodology employed to ascertain the structural integrity of ligands and their corresponding complexes. In the course of investigating the fragmentation patterns of L1 and

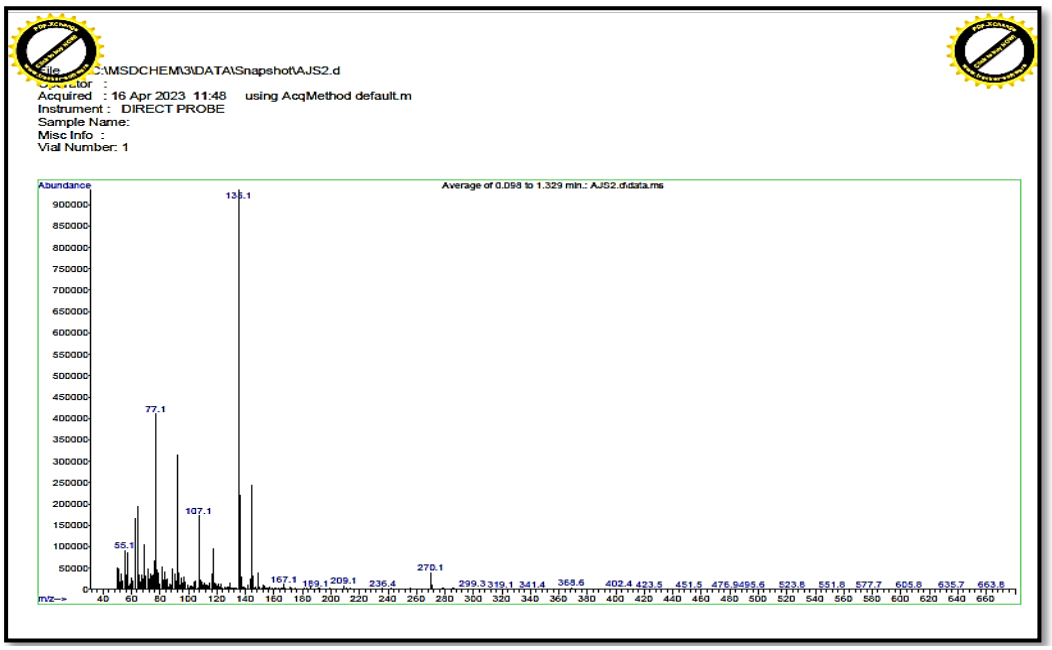

Fig. 6. Mass spectrum of azo ligand (5-MTADMBI).

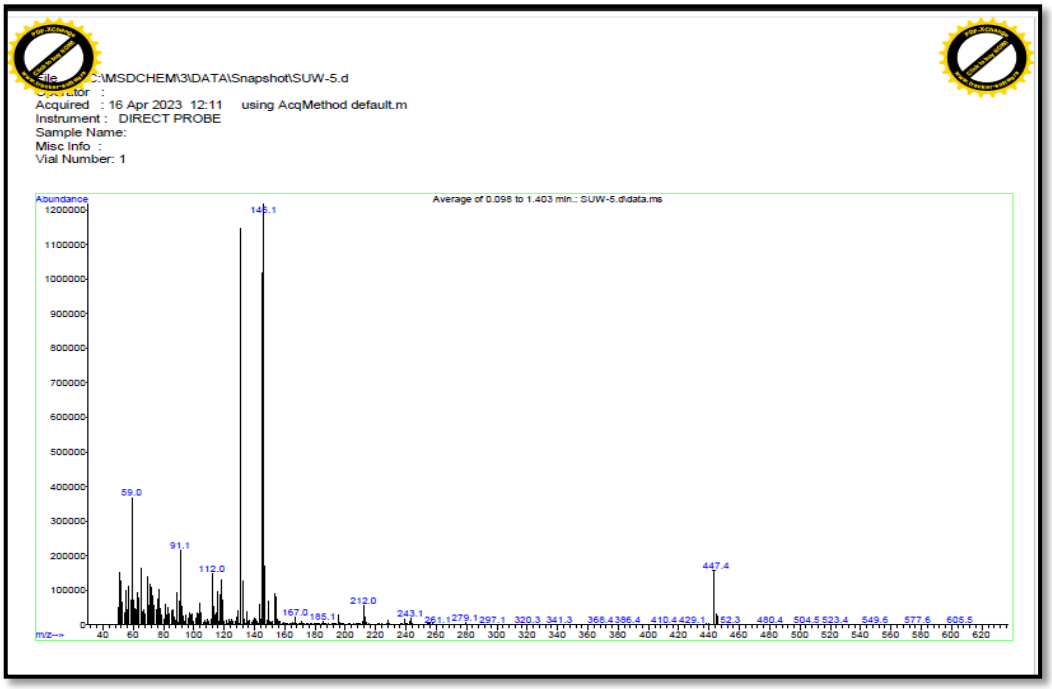

Fig. 7. Mass spectrum of Ag(I)-Complex.

C1, a multitude of signals were detected in the mass spectrum. Significantly, L1 exhibited a conspicuous base peak at m/z$^+$=270.1, which aligns with the authentic molar mass of L1 (271.34), featuring the chemical formula [$C_{13}H_{13}N_5S$]. Likewise, compound C1 prominently displayed a notable base peak at m/z$^+$=447.4, which aligns with its chemical formula (443.25) [$C_{13}H_{17}AgN_7O_2S$]. The observed experimental results exhibit excellent concordance with the anticipated chemical equations [25, 26]. The observed patterns pertaining to L1 and C1 are visually depicted in Figs. 6 and 7.

Infrared spectra of L_1 and its complexes

The infrared (IR) spectrum of L1 was subjected to comparative analysis with the spectra of various metal complexes in order to make predictions regarding the potential coordinating positions that might be implicated in the process of complexation. It is postulated that the positions and intensities of the bands in the spectra will undergo shifts upon the formation of a complex between the ligand and the metal ions [27-29]. The FT-IR spectral data of L1, as well as C1 and C2, are depicted in Fig. 8 and summarized in Table 3.

X-ray diffraction analysis

The X-ray diffraction (XRD) spectra of the compounds, in both their powdered and crystalline states, are depicted in Fig. 9. The experimental procedure involved the determination of the intensity of diffracted Cu-Kα radiation at various 2θ values spanning from 5° to 80°. This was accomplished by utilizing a K-alpha wavelength of

Table 3. The FT-IR frequencies (in cm^{-1}) data of ligand and metal complexes.

Group	Ligand	Au(III) Complex	Ag(II) Complex
υ - (OH)	-	3211-m.br	3363 m.br
υ - (CH_3)	2962 S.	2970 m.	2856 W.
-(C=N)υ	1614 br .S.	1589 br. S.	1612-1583 m.
-(N=N)υ	1477-1448 S.	1498-1473 s.	1502-1493 m.
-(C=C)υ	1708 m	1686 m	1676m
-(C-S)Thiaυ	1271 S.	1267 m.	1267 m.
υ-(C-N)Thia	1159 m.	1151 w.	1147 m.
υ(M-N)	-	615 m	607 W.

1.5406 Å and employing a generator setting of 30 mA/40 kV. The X-ray diffraction (XRD) values have been presented in Table 4. In order to determine the average size (D) of the crystallites in the samples, we employed the Scherer equation:

$$D = \frac{K\lambda}{\beta\cos\theta}$$

in the given expression, D symbolizes the average dimensions of the crystalline domains, β denotes the extent of diffraction peak broadening at half of its maximum intensity, k represents the Scherrer constant, which has been experimentally determined to be 0.891, θ corresponds to the Bragg's angle, and λ signifies the wavelength of X-rays [30-32]. Moreover, in order to determine the dislocation density, the mathematical expression 1/D2 was utilized. The experimental findings have elucidated that the dimensions of all the compounds were determined to be below 100 nanometers. The obtained results exhibit congruity with the observations derived from the field emission scanning electron microscopy (FE-SEM) analysis.

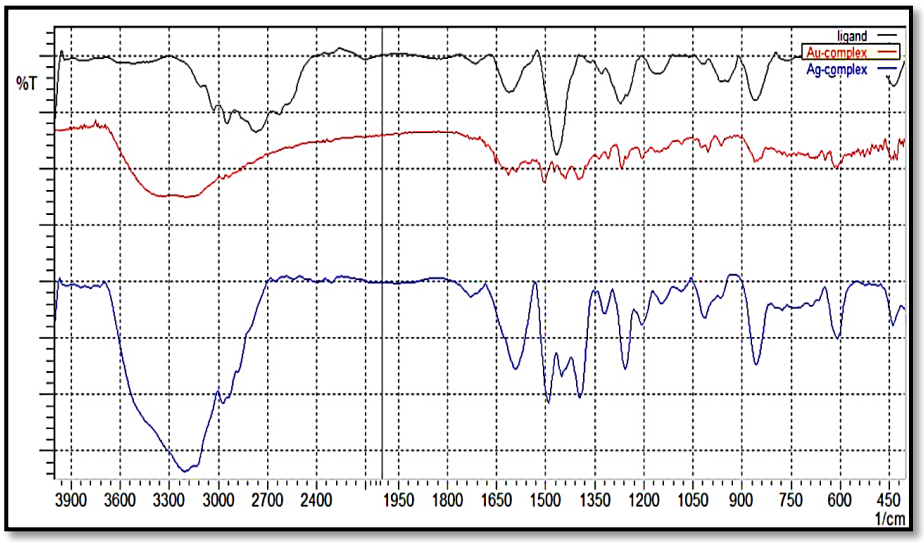

Fig. 8. FT-IR spectrum of the ligand (5-MTADMBI) and its metal complexes.

Table 4. Crystallographic data of the free ligand and metal complexes.

Compound	No.	°2Θ observed	d observed (A°)	(I/I·) %	FWHM	Crystallite Size. (nm)	(Lattice Strain)	$\delta_{DX10}{}^{15}$ (lin m^{-2})
(5-MTADMBI) $C_{13}H_{13}N_5S$	1	11.174	7.91228	100	0.184	45.33	0.0082	0. 486
	2	11.62	7.60720	22.13	0.16	52.15	0.0069	0.367
	3	9.86	8.96193	15.57	0.26	32.05	0.0132	0.973
	4	13.47	6.56662	8.49	0.24	34.83	0.0089	0.824
Ag (I) complex	1	16.261340	5.44646	100	0.208953	40.13	0.0064	0.620
	2	25.776470	3.45348	90.07	0.121369	70.16	0.0023	0.203
	3	22.382570	3.96887	78.45	0.104557	80.93	0.0023	0.152
	4	31.79	2.81258	71.83	0.12	71.93	0.0018	0.193
	5	9.03	9.78368	65.52	0.26	32.03	0.0144	0.974
Au (III) complex	1	26.303	3.38556	100	0.21	40.59	0.0039	0.606
	2	15.234	5.81127	86.57	0.18	46.53	0.0059	0.461
	3	34.326	2.61036	61.53	0.30	28.97	0.0042	1.19
	4	32.463	2.75580	59.39	0.12	72.05	0.0018	0.192
	5	24.625	3.61227	45.73	0.18	47.2	0.0036	0.448

FE-SEM Studies

The utilization of Field Emission Scanning Electron Microscopy (FE-SEM) was employed as a technique to thoroughly examine the L1 compound and its subsequent changes upon complexation to form C1 and C2. The primary focus of this investigation was directed toward analyzing the particle distribution, surface characteristics, and morphology of these compounds. The experimental investigation was conducted employing a cross-sectional distance of 200 nm and a magnification factor of 50,000KX. Fig. 10 displays an FE-SEM image depicting the compounds under investigation. The field emission scanning electron microscopy (FE-SEM) investigation unveiled the presence of L1 in the form of compact crystalline structures intricately intertwined, exhibiting an average particle size of 61.37 nm. In stark contrast, the C1 sample exhibited a remarkable homogeneity in its crystalline structure, extending uniformly throughout its entire surface area. The constituent particles, on average, displayed a size of precisely 73.52 nm. Ultimately, the field emission scanning electron microscopy (FE-SEM) analysis conducted on C2 unveiled the presence of sheet-like crystalline structures exhibiting a range of dimensions. Notably, the particles observed exhibited an average size of 50.24 nm, as reported in reference [33].

Antimicrobial activity

The concept of chelation is a highly valuable framework for comprehending the enhanced activity exhibited by metal complexes. Chelation is a fascinating phenomenon in which a metal ion and ligand molecules come together to create a remarkably stable ring-like structure. This unique arrangement results in a decrease in the polarity of metals, as the metal ion becomes enveloped by the ligands and forms what is known as a chelate. As a consequence, the positive charge residing on the metal ion is effectively shared and distributed among the various donor sites of the ligand. Moreover, in the course of this chemical transformation, the phenomenon of π-electron delocalization may manifest, thereby augmenting the inherent characteristics of the metal complex. One notable benefit of chelation is its ability to augment the lipophilicity of the metal chelate, facilitating its permeation through the lipoid layer of microorganisms, ultimately bolstering its efficacy in eradicating them. Activity can be enhanced by various factors, such as the solubility of the metal and ligand, the conductivity, and the bond length. In order to assess the activities of various samples, the inhibition zones, quantified in millimeters, were measured and are displayed in Table 5 and Fig. 11.

The utilization of the FE-SEM was employed as

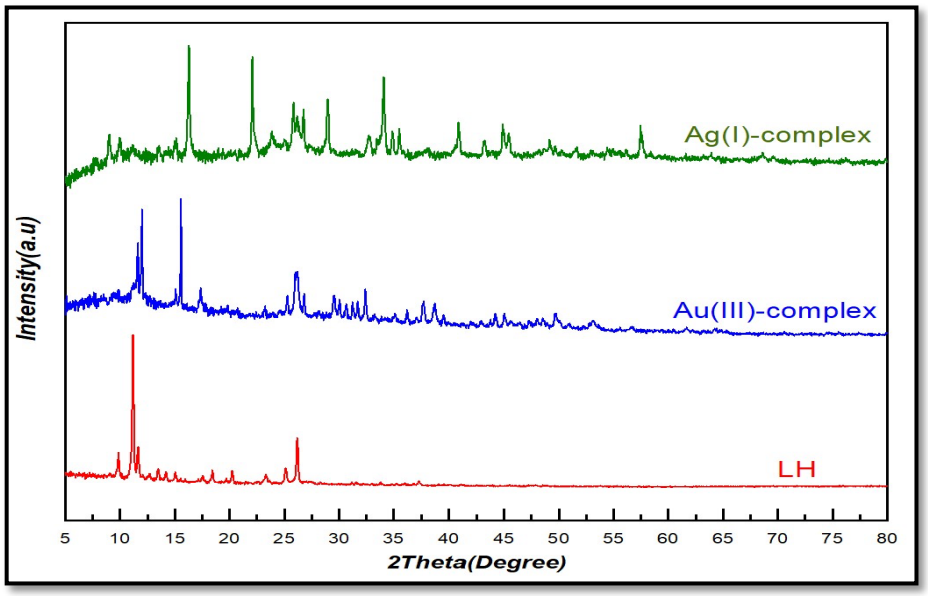

Fig. 9. XRD patterns for ligand (5-MTADMBI) and chelate complexes

a technique to explore the L1 and the subsequent alterations upon complexation, resulting in the formation of C1 and C2. The primary focus of this investigation was directed toward analyzing the particle distribution, surface characteristics, and morphology of these entities. The experimental investigation was conducted utilizing a cross-sectional separation of 200 nm and a magnification ratio of 50,000KX. Fig. 10 displays an FE-SEM image depicting the compounds under investigation. The FE-SEM investigation unveiled the presence of L1 in the form of compact crystalline structures

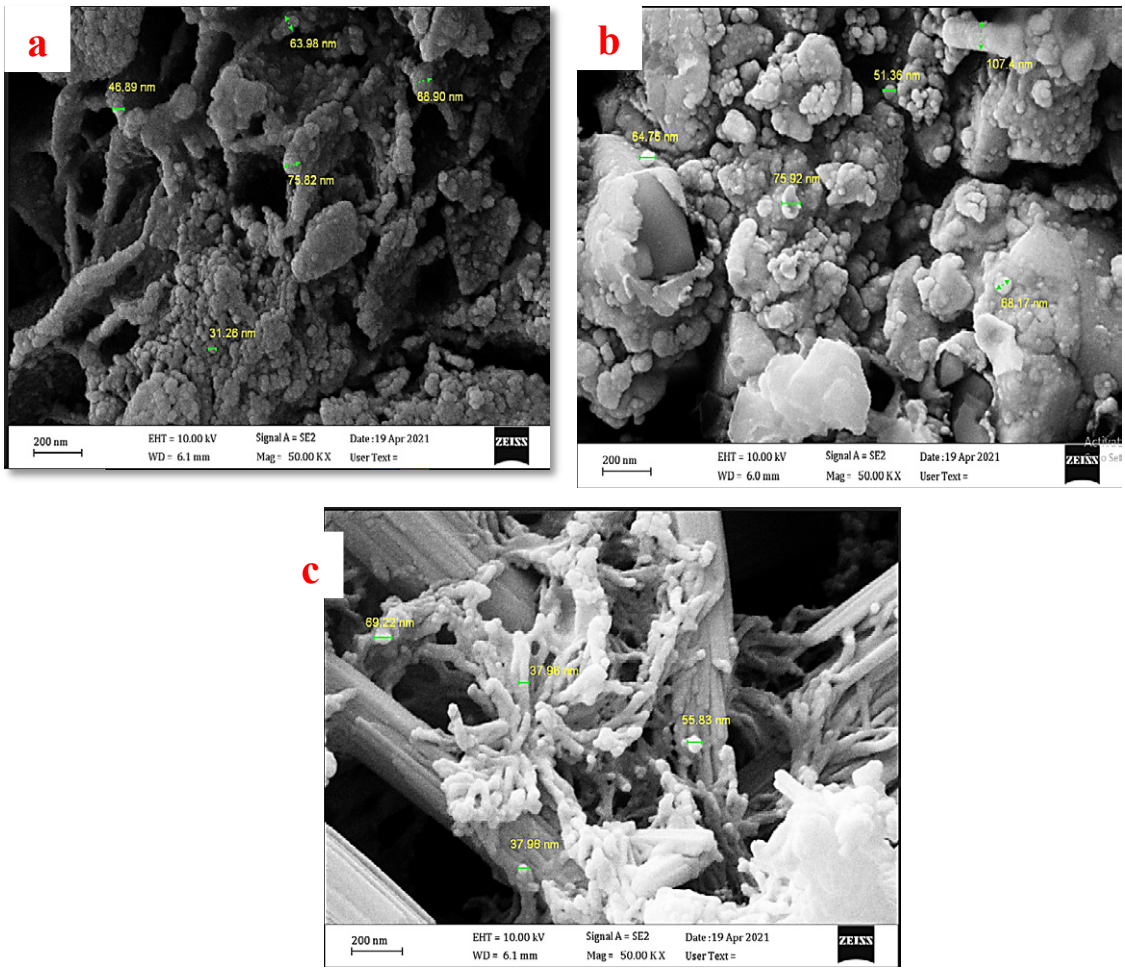

Fig. 10. FE-SEM images of (a) ligand(5-MTADMBI), (b) Ag(I)complex and (c) Au(III) complexes.

Table 5. Antimicrobial activity data for ligand and its metal complexes.

Compound	*Streptococcus*	*E.Coli*	*Penicillium sp.*
Ciprofloxacin	24	21	-
Cycloheximide	-	-	25
LH=(5-MTADMBI)	8	10	12
Ag(I) complex	15	14	17
Au(III) complex	16	14	18

(+++): high active—inhibition zone > 12 mm, (++): moderate active—inhibition zone = 9-12 mm (+): slightly active—inhibition zone = 6-9 mm, (-): inactive.

intricately intertwined, exhibiting an average particle size of 61.37 nm. In stark contrast, the C1 sample exhibited a remarkable homogeneity in its crystalline structure, extending uniformly throughout its entire surface area. The constituent particles, on average, manifested a size of precisely 73.52 nm. Ultimately, the FE-SEM analysis of C2 unveiled the presence of sheet-like crystalline structures exhibiting diverse dimensions, wherein the particles displayed an average size of 50.24 nm [33].

Cytotoxicity of L_1 and C_1 on TP-53 cell viability

Our investigation centered on assessing the efficacy of recently synthesized L1 and C1 compounds as prospective therapeutic agents for pancreatic carcinoma, in both metastatic and localized manifestations. The cytotoxic activity and mechanism of action against the TP-53 pancreas carcinoma cell line were investigated, and a comparative analysis was conducted with respect to their effects on normal human cells (HdFn) using the MTT assay. The duration of incubation

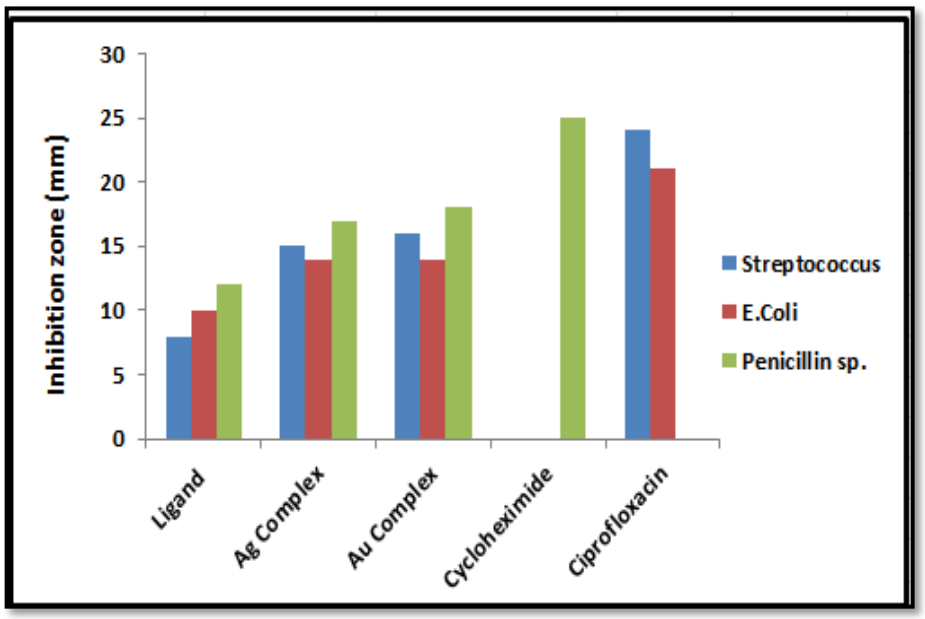

Fig. 11. Inhibition effect of the ligand and its complexes against microbial species.

Table 6. Evaluation of cytotoxicity of (5-MTADMBI) against TP-53 cancer cell line after incubation (24-hour) at (37 °C) and HdFn cell line.

Concentration (µg/mL)	5-MTADMBI			
	Cancer line cells		Normal line cells	
	TP-53	% Cell Inhibition	HdFn	% Cell Inhibition
	Cell Viability (Mean ±SD)		Cell Viability (Mean ±SD)	
200	39.12±3.15	60.88	62.26±4.62	37.74
100	27.66±2.27	72.34	71.142±1.83	28.858
50	54.012±3.23	45.99	65.97±1.10	34.03
25	64.69±4.71	35.31	86.304±3.74	13.696
12.5	75.038±4.9	24.962	95.37±0.90	4.63

Table 7. Evaluation of cytotoxicity of (Ag-Complex) against TP-53 cancer cell line after incubation (24-hour) at (37 °C) and HdFn cell line.

Concentration (µg/mL)	Ag-Complex			
	Cancer line cells		Normal line cells	
	TP-53	% Cell Inhibition	HdFn	% Cell Inhibition
	Cell Viability		Cell Viability	
	(Mean ±SD)		(Mean ±SD)	
200	51.81±0.40	48.19	80.20±3.11	19.80
100	41.39±5.75	58.61	85.64±3.3	14.36
50	61.96±4.38	38.04	72.64±1.9	27.36
25	73.2±2.71	26.80	94.17±0.77	5.83
12.5	84.14±0.83	15.86	96.18±0.23	3.82

was observed to be 24 hours at a temperature of 37°C, while a series of concentration ranges, specifically 0.0125, 0.025, 0.050, 0.100, and 0.200 mg/mL, were subjected to experimental analysis [42,43].

The experimental findings elucidated that when administered at a concentration of 100 µg/ml, both L1 and C1 demonstrated pronounced inhibitory properties towards tumor cell demise, manifesting cytotoxicity levels of 72.34% and 58.61%, respectively. Nevertheless, it is noteworthy that the normal cells (referred to as HdFn) exhibited a significant inhibition rate of 28.85% and 14.36% at the identical administered dosage. It is intriguing to note that the optimal suppression of both cancer cells and normal cells was achieved at a concentration of 100 µg/ml during a 24-hour incubation period, whereas minimal inhibition was observed at concentrations of 12.5 µg/ml. The concentration denoted as the IC50, or half maximal inhibitory concentration, corresponds to the concentration at which approximately 50% of the cellular population is effectively eradicated [44]. The selective cytotoxic potential of L1 against TP-53 pancreas cancer cells was observed with an IC50 value of 11.92 µM/ml. In contrast, the IC50 value for normal human cells (HdFn) was determined to be 76.85 µM/ml. In a similar fashion, compound C1 exhibited a remarkable phenomenon of selective cytotoxicity

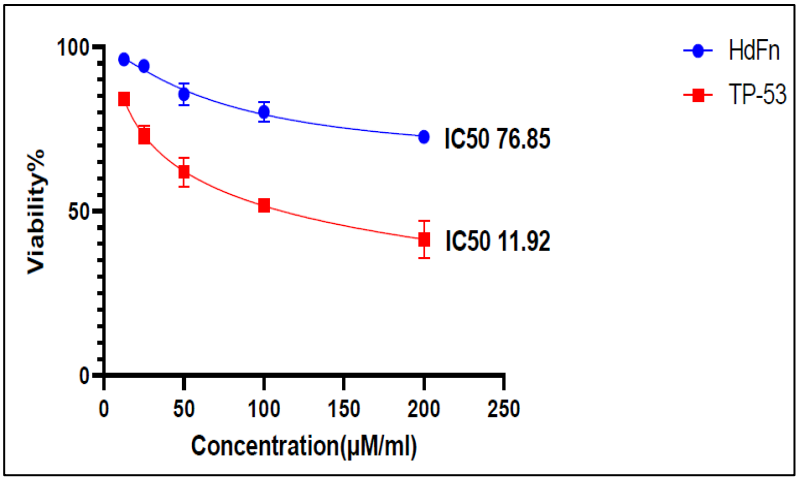

Fig. 12. IC_{50} for ligand (5-MTADMBI) in (TP-53) cell line and (HdFn) natural cell line

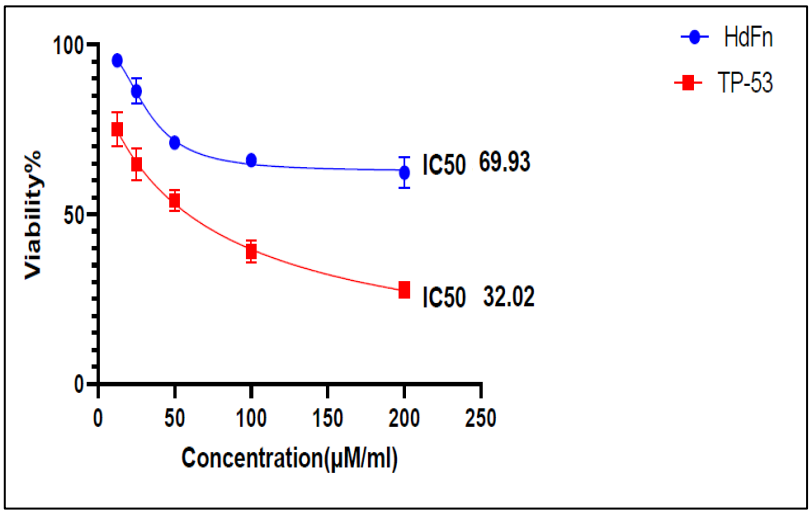

Fig. 13. IC_{50} for Ag(I)-Complex in (TP-53) cell line and (HdFn) natural cell line

towards TP-53 pancreas cancer cells, as evidenced by its IC50 value of 32.02 µM/ml. In stark contrast, the IC50 value for normal human cells (HdFn) was determined to be 69.93 µM/ml. The results of this study indicate that the synthesized compounds exhibit considerable potential as prospective antitumor agents within the realm of medical science and pharmaceutical applications, particularly in the context of pancreatic cancer treatment. The experimental results pertaining to the viability rates of different compound dosages administered to TP-53 and HdFn cells for a duration of 24 hours, as well as the corresponding IC50 values, are displayed in Tables 6 and 7, respectively. The experimental data presented in Figs. 13 and 14 depict the viability rate of TP-53 cells and HdFn cells upon exposure to the aforementioned compounds.

Molecular docking calculation

The comparative evaluation of the biological potentials of the synthesized compounds was conducted through molecular docking studies against proteins associated with pancreatic cancer. The potential of the compound against these proteins is influenced by several factors, with the interaction between the synthesized compound and the proteins being the most prominent determinant. The observed activity exhibited enhancement as a consequence of the progressive strengthening of the intermolecular interactions between the compounds and the proteins. During the docking process, it was observed that four distinct categories of chemical interactions manifested, namely hydrogen bonding, p-p interactions, hydrophobic interactions, and interactions facilitated by halogens [36-38].

In Fig. 10, a multitude of parameters derived from the intricate intermolecular interactions are elegantly showcased. Significantly, upon the interaction of L1 with the pancreatic cancer protein (6HP9), the establishment of hydrogen bonding occurred between the (S15 atom, N16 atom, and 6-ring molecule) and the amino acids GLU 672, GLU 672, and PHE 785, correspondingly. The compounds exhibited both polar and hydrophobic interactions with the adjacent proteins. Upon the interaction of compound C1 with the pancreatic cancer protein (6HP9), a series of intermolecular interactions take place. These interactions involve three types: hydrogen bonding, specifically involving hydrogen donors and acceptors, as well as ionic interactions. Specifically, the atoms S15, O18, O19, O18, and Ag17 engage in these interactions with the amino acids VAL 763, ASP 784, HIS 764, ARG 765, and ARG 765, respectively. Furthermore, the C2 moiety established both ionic and pi-H interactions within the (6HP9) protein through its interaction with the Au17 atom and the 5-ring molecule, specifically with ARG 765 and ILE 675 residues.

In the realm of computational chemistry, it is noteworthy to mention that several crucial parameters are derived from these calculations.

These parameters encompass Glide H-bond, Glide evdw, and Glide ecoul, each of which assumes a pivotal role in elucidating the intricate intermolecular interactions between synthesized compounds and proteins [39]. Furthermore, the analysis of the synthetic compounds and proteins involved the utilization of various parameters such as the Glide e-model, Glide energy, Glide einternal, and Glide posenum to assess their interactions.

CONCLUSION

The synthesis and structural characterization of the azo dye ligand (5-MTADMBI) derived from thiazole, along with its Ag(I) and Au(III) complexes, have been successfully accomplished. The structures of the synthesized compounds have been confirmed through the utilization of elemental analysis (C.H.N.S), mass spectrometry, ^{1}H NMR, ^{13}C NMR, FT-IR, magnetic susceptibility measurements, and molar conductivity measurements. The utilization of XRD and FE-SEM methodologies have substantiated the distinct morphological characteristics exhibited by the ligand and its corresponding metal complexes. The optimization of the molecular structure of the complexes has been achieved through the analysis of the spectral data. Based on these findings, it has been suggested that the Ag(I)-Complex adopts a tetrahedral geometry, characterized by sp^3 hybridization. On the other hand, the proposed geometry for the Au(III)-Complex is a square planar arrangement, which is indicative of d_{sp2} hybridization. The biological activity entailed the execution of cell viability and cytotoxicity assays on the ligand (5-MTADMBI) and Ag(I) complexes. This was accomplished by employing the lines of the pancreas carcinoma cell line (TP-53) and normal human cells (HdFn) for comparison. From the results, it can be deduced that the azo ligand and Ag(I) Complex exhibit favorable cytotoxic characteristics and selectivity towards the pancreas carcinoma cell line (TP-53) cells.

CONFLICT OF INTEREST

The authors declare that there is no conflict of interests regarding the publication of this manuscript.

REFERENCES

1. Kyhoiesh HAK, Al-Adilee KJ. Synthesis, spectral characterization, antimicrobial evaluation studies and cytotoxic activity of some transition metal complexes with tridentate (N,N,O) donor azo dye ligand. Results in Chemistry. 2021;3:100245.
2. Hossain M. A Review on Heterocyclic: Synthesis and Their Application in Medicinal Chemistry of Imidazole Moiety. Science Journal of Chemistry. 2018;6(5):83.
3. Viji A, Balachandran V, Babiyana S, Narayana B, Salian VV. FT-IR and FT-Raman investigation, quantum chemical studies, molecular docking study and antimicrobial activity studies on novel bioactive drug of 1-(2,4-Dichlorobenzyl)-3-[2-(3-(4-chlorophenyl)-5-(4-(propan-2-yl)phenyl-4,5-dihydro-1H-pyrazol-1-yl]-4-oxo-4,5-dihydro-1,3-thiazol-5(4H)-ylidence]-2,3-dihydro-1H-indol-2-one. Journal of Molecular Structure. 2020;1215:128244.
4. Waheeb AS, Al-Adilee KJ. Synthesis, characterization and antimicrobial activity studies of new heterocyclic azo dye derived from 2-amino- 4,5- dimethyl thiazole with some metal ions. Materials Today: Proceedings. 2021;42:2150-2163.
5. Witwit IN, Mubark HMH, Ali AAM. Synthesis and studying the coordination behavior of a new heterocyclic imidazole azo ligand with some of the first series transition and (IIB) ions. International conference of numerical analysis and applied mathematics icnaam 2019: AIP Publishing; 2020.
6. Karam F, hessoon h. Synthesis, identification, biological activity and anti-cancer activity Studies of Hetrocyclic Ligand Azo-schiff Base with Au(III) Complex. Egyptian Journal of Chemistry. 2021;0(0):0-0.
7. Rai HS, Bhattacharyya MS, Singh J, Bansal TK, Vats P, Banerjee UC. Removal of Dyes from the Effluent of Textile and Dyestuff Manufacturing Industry: A Review of Emerging Techniques With Reference to Biological Treatment. Crit Rev Environ Sci Technol. 2005;35(3):219-238.
8. Deshmukh SP, Patil SM, Mullani SB, Delekar SD. Silver nanoparticles as an effective disinfectant: A review. Materials Science and Engineering: C. 2019;97:954-965.
9. Soliman AM, Karam HM, Mekkawy MH, Ghorab MM. Antioxidant activity of novel quinazolinones bearing sulfonamide: Potential radiomodulatory effects on liver tissues via NF-κB/ PON1 pathway. Eur J Med Chem. 2020;197:112333.
10. Harisha S, Keshavayya J, Prasanna SM, Joy Hoskeri H. Synthesis, characterization, pharmacological evaluation and molecular docking studies of benzothiazole azo derivatives. Journal of Molecular Structure. 2020;1218:128477.
11. Bhutani R, Pathak DP, Kapoor G, Husain A, Kant R, Iqbal MA. Synthesis, molecular modelling studies and ADME prediction of benzothiazole clubbed oxadiazole-Mannich bases, and evaluation of their anti-diabetic activity through in vivo model. Bioorg Chem. 2018;77:6-15.
12. Al-Adilee KJ, Abedalrazaq KA, Al-Hamdiny ZM. Synthesis and Spectroscopic Properties of Some Transition Metal Complexes with New Azo-Dyes Derived From Thiazole and Imidazole. Asian J Chem. 2013;25(18):10475-10481.
13. Park J-A, Lee JW, Kim H-K, Shin UC, Lee KC, Kim T-J, et al. Radiometallic Complexes of DO3A-Benzothiazole Aniline for Nuclear Medicine Theranostics. Mol Pharm. 2018;15(3):1133-1141.
14. Law SK. Medical Treatment: Carbonic Anhydrase Inhibitors. Pearls of Glaucoma Management: Springer Berlin Heidelberg; 2009. p. 207-211.
15. Saeed S, Rashid N, Jones PG, Ali M, Hussain R. Synthesis, characterization and biological evaluation of some thiourea derivatives bearing benzothiazole moiety as potential antimicrobial and anticancer agents. Eur J Med Chem.

2010;45(4):1323-1331.
16. Al-Adilee KJ, Hasan SR. Synthesis, Characterization and Biological Activity of Heterocyclic Azo-Schiff Base Ligand derived from 2-Amino-5-methyl thiazol and some Transition Metal Ions. IOP Conference Series: Earth and Environmental Science. 2021;790(1):012031.
17. Kyhoiesh HAK, Al-Adilee KJ. Synthesis, spectral characterization and biological activities of Ag(I), Pt(IV) and Au(III) complexes with novel azo dye ligand (N, N, O) derived from 2-amino-6-methoxy benzothiazole. Chemical Papers. 2022;76(5):2777-2810.
18. Mabrouk M, Hammad SF, Abdelaziz MA, Mansour FR. Ligand exchange method for determination of mole ratios of relatively weak metal complexes: a comparative study. Chem Cent J. 2018;12(1).
19. Zhu B, Raza R, Qin H, Liu Q, Fan L. Fuel cells based on electrolyte and non-electrolyte separators. Energy & Environmental Science. 2011;4(8):2986.
20. Fei G, Pin Y, Jun X, Hongfei W. Synthesis, characterization and antibacterial activity of novel Fe(III), Co(II), and Zn(II) complexes with norfloxacin. J Inorg Biochem. 1995;60(1):61-67.
21. Al-Adilee K, Dakheel H. Synthesis, Spectral and Biological Studies of Ni(II), Pd(II), and Pt(IV) Complexes with New Heterocyclic ligand Derived from Azo-Schiff Bases Dye. Eurasian Journal of Analytical Chemistry. 2018;13(6).
22. Al-Saif FA. Spectroscopic Elucidation, Conductivity and Activation Thermodynamic Parameters Studies on Pt(IV), Au(III) and Pd(II) 1,5-Dimethyl-2-phenyl-4-[(thiophen-2-ylmethylene)- amino]-1,2-dihydro-pyrazol-3-one Schiff Base Complexes. International Journal of Electrochemical Science. 2014;9(1):398-417.
23. Al-Adilee KJ, Jaber SA. Synthesis, Characterization and Biological Activities of Some Metal Complexes Derived from Azo Dye Ligand 2-[2'-(5-Methyl thiazolyl) azo]-5-dimethylamino Benzoic Acid. Asian J Chem. 2018;30(7):1537-1545.
24. Waheeb AS. Spectroscopic, characterization and bioactivity studies of new Ni (II), Cu (II) and Ag (I) complexes with didentate (N,N) donar azo dye ligand. Journal of Molecular Structure. 2023;1276:134729.
25. Chandra S, Gupta LK. Electronic, EPR, magnetic and mass spectral studies of mono and homo-binuclear Co(II) and Cu(II) complexes with a novel macrocyclic ligand. Spectrochimica Acta Part A: Molecular and Biomolecular Spectroscopy. 2005;62(4-5):1102-1106.
26. Al-Adilee KJ, Abass AK, Taher AM. Synthesis of some transition metal complexes with new heterocyclic thiazolyl azo dye and their uses as sensitizers in photo reactions. Journal of Molecular Structure. 2016;1108:378-397.
27. J. Al-Adilee K, Adnan S. Synthesis and Spectral Properties Studies of Novel Hetrocyclic Mono Azo dye Derived from Thiazole and Pyridine with Some Transition Complexes. Oriental Journal of Chemistry. 2017;33(04):1815-1827.
28. Ali Shihad AA, Hessoon HM, Karam FF, Al-Adilee KJ. Novel method for determination of Zinc in some pharmaceutics using new prepared reagent of methyl phenol. IOP Conference Series: Earth and Environmental Science. 2021;790(1):012010.
29. Serafińczuk J, Moszak K, Pawlaczyk Ł, Olszewski W, Pucicki D, Kudrawiec R, Hommel D. Determination of dislocation density in GaN/sapphire layers using XRD measurements carried out from the edge of the sample. Journal of Alloys and Compounds. 2020;825:153838.
30. Venugopal N, Krishnamurthy G, Bhojyanaik HS, Murali Krishna P. Synthesis, spectral characterization and biological studies of Cu (II), Co (II) and Ni (II) complexes of azo dye ligand containing 4-amino antipyrine moiety. Journal of Molecular Structure. 2019;1183:37-51.
31. El-Boraey HA, El-Domiaty AM. Influences of γ-ray irradiation on physico-chemical, structural, X-ray diffraction, thermal and antimicrobial activity of some γ-irradiated N′,N‴-((Z)-ethane-1,2-diylidine)bis(2-aminobenzohydrazide) metal complexes. Applied Radiation and Isotopes. 2021;174:109774.
32. Marulanda Cardona DM, Wongsa-Ngam J, Jimenez H, Langdon TG. Effects on hardness and microstructure of AISI 1020 low-carbon steel processed by high-pressure torsion. Journal of Materials Research and Technology. 2017;6(4):355-360.
33. Tyuftin AA, Mohammed H, P. Kerry J, O'Sullivan MG, Hamill R, Kilcawley K. Microscopy-Assisted Digital Photography as an Economical Analytical Tool for Assessment of Food Particles and Their Distribution Through The use of the ImageJ Program. Advances in Nutrition and Food science. 2021;2021(02).
34. Al-Adilee KJ, Waheeb AS. Preparation, spectroscopic and anticancer studies of metal antibiotic Chelation Ni(II), Cu(II) and Zn(II) 4,5-dimethyl Thiazolylazo complexes. Journal of Physics: Conference Series. 2020;1664(1):012057.
35. Azam M, Mohammad Wabaidur S, Alam M, Trzesowska-Kruszynska A, Kruszynski R, Al-Resayes SI, et al. Design, structural investigations and antimicrobial activity of pyrazole nucleating copper and zinc complexes. Polyhedron. 2021;195:114991.
36. Liu D, Enriquez L, Ford CE. ROR2 Is Epigenetically Regulated in Endometrial Cancer. Cancers (Basel). 2021;13(3):383.
37. Ying X, Che X, Wang J, Zou G, Yu Q, Zhang X. CDK1 serves as a novel therapeutic target for endometrioid endometrial cancer. J Cancer. 2021;12(8):2206-2215.
38. Al-adilee KJ, Hessoon HM. Synthesis, Spectral Properties And Anticancer Studies of Novel Hetrocyclic Azo Dye Ligand Derived From 2-Amino-5-methyl thiazole with Some Transition Metal Complexes. Journal of Physics: Conference Series. 2019;1234(1):012094.
39. Johnatty SE, Pesaran T, Dolinsky J, Yussuf A, LaDuca H, James PA, et al. Case–case analysis addressing ascertainment bias for multigene panel testing implicates BRCA1 and PALB2 in endometrial cancer. Hum Mutat. 2021;42(10):1265-1278.